Journal of Alloys and Compounds 384 (2004) 25–32

Journal of ALLOYS AND COMPOUNDS

www.elsevier.com/locate/jallcom

Mössbauer effect studies of $Dy(Mn_{0.4-x}Al_xFe_{0.6})_2$ compounds

P. Stoch [a], J. Pszczoła [a,*], P. Guzdek [a], M. Wzorek [a], A. Jabłońska [b], J. Suwalski [b], L. Dąbrowski [b], A. Pańta [c]

[a] *Solid State Physics Department, AGH, Al. Mickiewicza 30, 30-059 Kraków, Poland*
[b] *Institute of Atomic Energy, 05-400 Świerk-Otwock, Poland*
[c] *Department of Metallurgy and Materials Engineering, AGH, Al. Mickiewicza 30, 30-059 Kraków, Poland*

Received 26 February 2004; received in revised form 24 March 2004; accepted 24 March 2004

Abstract

It was previously found that the magnetic hyperfine fields observed at ^{57}Fe nuclei (4.2 K) in the $Dy(Mn_{1-x}Fe_x)_2$ and $Dy(Fe_{1-x}Co_x)_2$ intermetallics form a Slater–Pauling curve. Both 3d subbands in the $Dy(Mn_{0.4}Fe_{0.6})_2$ compound are filled up only partially with 3d electrons. The consequence of Mn/Al substitution, in the $Dy(Mn_{0.4}Fe_{0.6})_2$ compound was studied in the present paper. For this purpose the synthesis and X-ray analysis (300 K) of the series $Dy(Mn_{0.4-x}Al_xFe_{0.6})_2$ were performed. The cubic, $MgCu_2$-type Fd3m crystal structure was observed across the series. Nevertheless for $x = 0.35$ and 0.40 a stoichiometric admixture of the hexagonal, $MgZn_2$-type, $P6_3$/mmc was evidenced. ^{57}Fe Mössbauer effect measurements for the series were performed at 4.2 K. The magnetic hyperfine fields form a separate branch of the Slater–Pauling curve. This branch is compared to the magnetic hyperfine field previously obtained for the $Dy(Mn_{0.4}Fe_{0.6-x}Al_x)_2$ series (the Fe/Al substitution). The possible 3d electron band structure is discussed qualitatively within the Stoner model.

Keywords: Intermetallics; Crystal structure; ^{57}Fe Mössbauer effect; Hyperfine interactions; Slater–Pauling curve; Band structure

1. Introduction

Fundamental interest and practical applications are the reason behind the numerous studies of the heavy rare earth (R)–transition metal (M) compounds [1–3]. The ferrimagnetism of the R–M compounds results from the coexistence between the 4f (5d) and 3d electron magnetism [4–6]. It was previously found that the magnetic properties of the R-M materials are mainly governed by the 3d electrons of the transition metal sublattice [4–6]. However, the electronic band structure of the R–M intermetallics, especially of their transition metal constituent, is rather complex and poorly known up to date.

Systematic Mössbauer effect studies of the substituted RM_2 series of compounds were a useful method to test both the rare earth and the transition metal sublattice and thus to clarify the 3d–5d–4f magnetism [5]. In particular, it was previously found that the magnetic hyperfine fields $\mu_0 H_{hf}$ (μ_0 is the magnetic permeability), determined at ^{57}Fe nuclei in the $Dy(Mn_{1-x}Fe_x)_2$ and $Dy(Fe_{1-x}Co_x)_2$ intermetallic series, treated as a function of the average number n of 3d electrons calculated per transition metal site (in analogy to the 3d metal–3d metal alloys [7–9]) behave according to the Slater–Pauling curve with a maximum hyperfine field appearing for the $Dy(Fe_{0.7}Co_{0.3})_2$ compound [5,6].

Across the $Dy(Mn_{1-x}Fe_x)_2$ series the 3d subbands are filled-up step by step and consequently the magnetic hyperfine field $\mu_0 H_{hf}$ increases with x (or n) [5]. It can be noticed that in this series no one 3d subband approaches its completeness.

Al substitution is a widely used method to modify 3d bands and thus to modify the magnetic properties and hyperfine interactions, as for instance in Refs. [10,11]. Al atom substituted into the M sublattice introduces the $3s^2p^1$ electrons instead of the $3d^64s^2$ electrons of iron atom or $3d^54s^2$ electrons of manganese atom. This replacing strongly influences the 3d band and thus the magnetism and hyperfine interactions of the compounds [10–15].

The significance of the iron component was studied recently using Fe/Al substitution in the series $Dy(Mn_{0.4}Fe_{0.6-x}Al_x)_2$ (the 3d subbands are populated only partially) [16].

* Corresponding author.
E-mail address: pszczola@uci.agh.edu.pl (J. Pszczoła).

0925-8388/$ – see front matter © 2004 Elsevier B.V. All rights reserved.
doi:10.1016/j.jallcom.2004.03.123

It would be interesting to study, for a comparison, the significance of the manganese component in the compounds, with the 3d subbands only partially occupied by 3d electrons. Thus to test the influence of the manganese atoms on the 4f–5d–3d magnetism and especially on the magnetism of the 3d sublattice, Mn/Al substitution in the $Dy(Mn_{0.4-x}Al_xFe_{0.6})_2$ series was used in the present paper.

The compounds $Dy(Mn_{0.4-x}Al_xFe_{0.6})_2$ were synthesized and subsequently X-ray and ^{57}Fe Mössbauer effect measurements were performed. The obtained data are qualitatively discussed within the frame of the rigid band model [9,17,18].

2. Materials and crystal structure

New intermetallics $Dy(Mn_{0.4-x}Al_xFe_{0.6})_2$ ($x = 0$, 0.05, 0.10, 0.15, 0.20, 0.25, 0.30, 0.35 and 0.40) were prepared by arc melting, in a high-purity argon atmosphere from the appropriate amounts of Dy (99.9% purity), Mn, Fe and Al (all 99.99% purity) as starting materials.

The X-ray patterns obtained for these compounds (Fig. 1) were analyzed using the Rietveld-type procedure [19,20]. The cubic, Fd3m, $MgCu_2$-type (C15) Laves phases [21–23] were observed across the series. Nevertheless, for $x = 0.35$ and 0.40 an admixture (presumably stoichiometric) of the

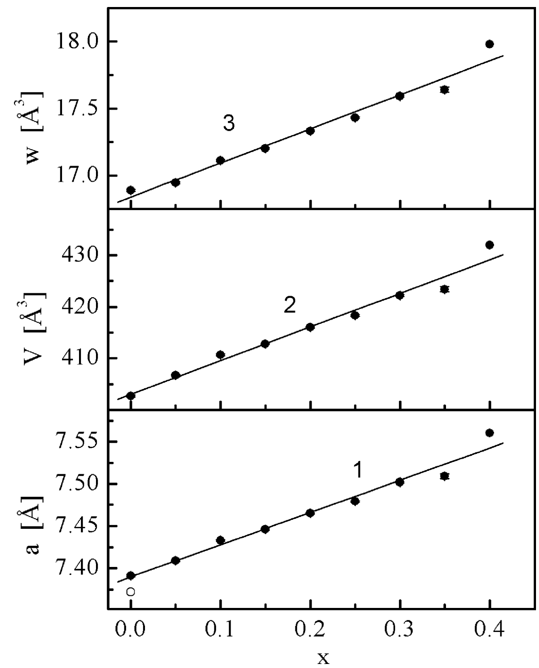

Fig. 2. The crystal lattice parameters of the $Dy(Mn_{0.4-x}Al_xFe_{0.6})_2$ intermetallics (300 K) for the $MgCu_2$-type structure: (1) the lattice edge a, (2) the unit cell volume V and (3) the volume w calculated per atom.

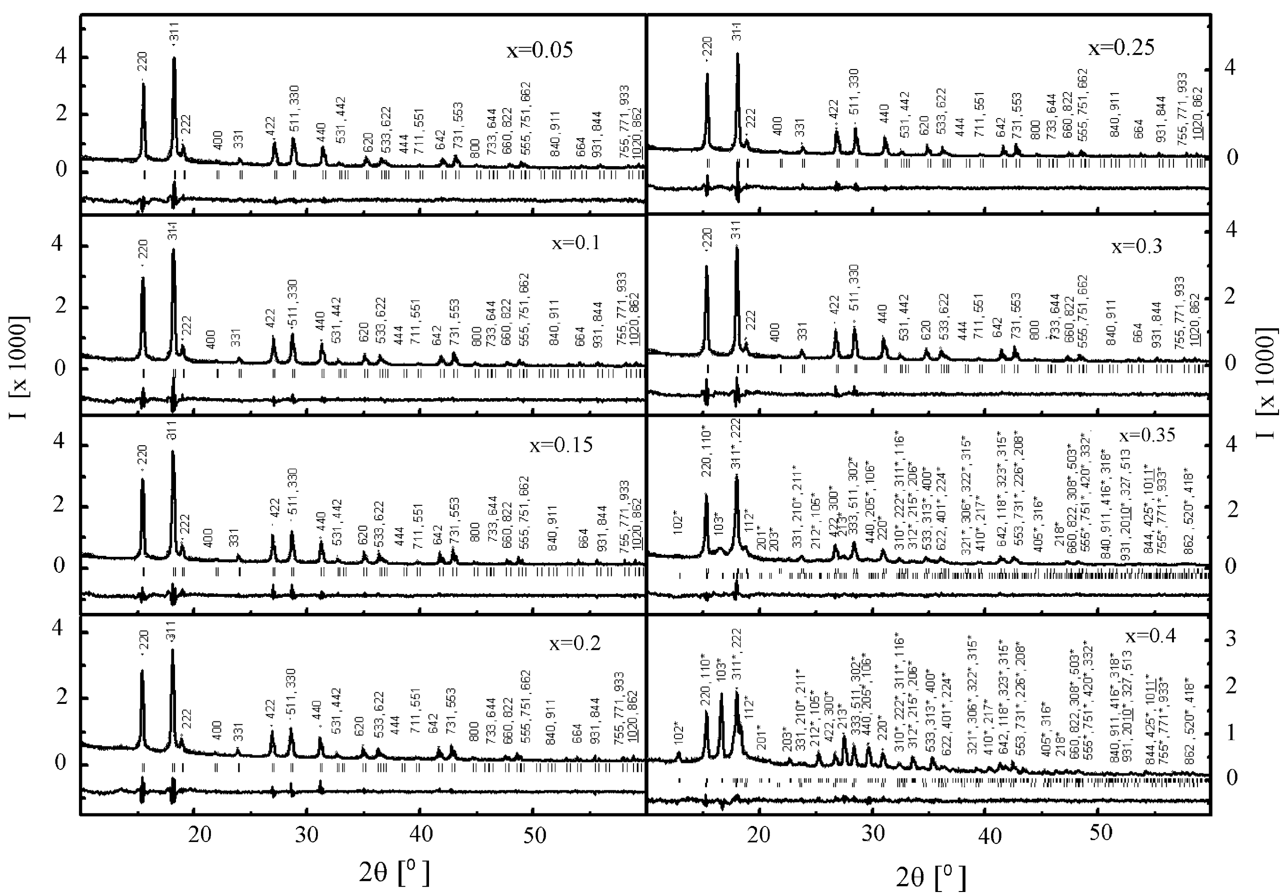

Fig. 1. X-ray powder diffraction patterns observed for the $Dy(Mn_{0.4-x}Al_xFe_{0.6})_2$ intermetallics (300 K). Asterisk denotes the second crystallographic phase in the mixed region. Fitted differential pattern is added below each diffractogram.

Table 1
Crystallographic data for the $Dy(Mn_{0.4-x}Al_xFe_{0.6})_2$ series (300 K)

x	Phase (%)	a (Å)	c (Å)	V (Å^3)	w (Å^3)
$MgCu_2$-type phase					
0	100	7.391(1); 7.372(2) [25]		403.7(5)	16.89(2)
0.05	100	7.409(1)		406.7(2)	16.94(1)
0.10	100	7.433(1)		410.7(2)	17.11(1)
0.15	100	7.4461(8)		412.8(1)	17.20(1)
0.20	100	7.4649(8)		416.0(1)	17.33(1)
0.25	100	7.4793(9)		418.4(2)	17.43(1)
0.30	100	7.502(1)		422.2(2)	17.59(1)
0.35	58(2)	7.509(3)		423.4(5)	17.64(2)
0.40	32(3)	7.560(1)		432(2)	17.98(7)
$MgZn_2$-type phase					
0.35	42(2)	5.328(1)	8.630(1)	212.2(4)	17.68(3)
0.4	68(3)	5.319(1); 5.319(3) [13]	8.683(1); 8.686(2)	212.8(4); 212.8(5)	17.73(3); 17.73(4)

a, c: unit cell parameters; V: unit cell volume; w: volume per atom.

hexagonal, $P6_3mmc$, $MgZn_2$-type (C14) Laves phase can be observed. A possible coexistence of the stoichiometric similar C14 and C15 Laves phases in the compound was previously discussed elsewhere [24].

For further practical reasons, it is worth noticing that the $MgCu_2$-type unit cell contains eight stoichiometric formula units, i.e. 24 atoms: 8 Mg and 16 Cu atoms. Each Cu (or transition metal atom M) has six Cu (or M) atoms in the nearest neighbor shell (radius: $a(2)^{1/2}/4$) [21,22].

The lattice parameters a and c obtained from the fitting procedure, the unit cell volume V and the volume w per atom are presented in Table 1 (the value at $x = 0$ estimated from data of the $Dy(Mn_{1-y}Fe_y)_2$ series [25] and the value for $x = 0.4$ are added [13]). Moreover the a, V and w data for the $MgCu_2$-type of structure are presented in Fig. 2. In practice the Vegard rule is obeyed and thus a linear dependence for the $a(x)$ parameter, described by the numerical formula $a(x) = [0.352(13)x + 7.393(3)]$ Å^3, is observed.

3. Spectra and analysis

The Mössbauer effect measurements were performed at 4.2 K by using a standard transmission technique with a source of ^{57}Co in Rh.

The experimental ^{57}Fe Mössbauer effect spectra (points) observed for the $Dy(Mn_{0.4-x}Al_xFe_{0.6})_2$ series (x = 0, 0.05, 0.10, 0.15, 0.20 and 0.30) are presented in Fig. 3. As these spectra are composed of a number of subspectra they are weakly resolved. This complexity should be mainly related to the different, presumably random {Mn, Al, Fe} nearest neighbor (n.n.) surroundings of the observed Fe atom resulting from the Mn/Al substitution. Each {Mn, Al, Fe} n.n. surrounding introduces its own subspectrum and thus its own set of hyperfine interaction parameters. Following formula $Dy(Mn_{0.4-x}Al_xFe_{0.6})_2$ it can be noticed that there are probabilities $p_1 = (0.4 - x)$, $p_2 = x$ and $p_3 = 0.6$ to find in the crystal lattice the Mn, Al and Fe atom, respectively.

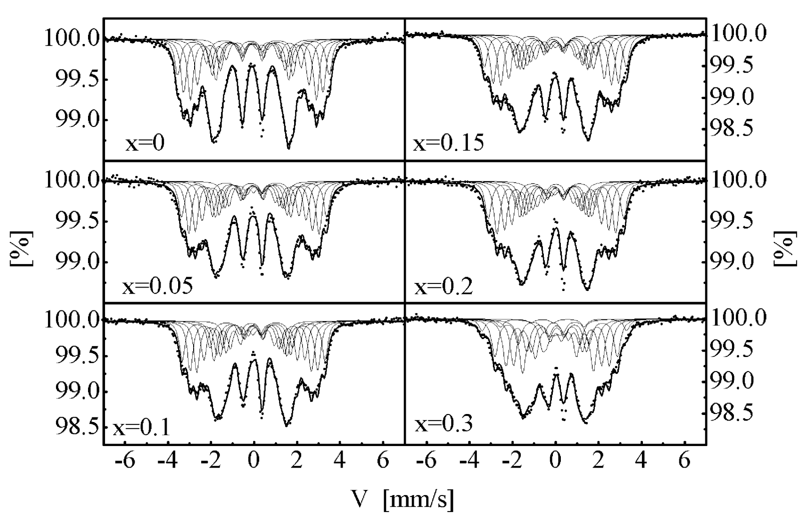

Fig. 3. ^{57}Fe Mössbauer effect transmission spectra of the $Dy(Mn_{0.4-x}Al_xFe_{0.6})_2$ intermetallics (4.2 K). Experimental points, fitted lines and fitted subspectra are presented.

Table 2
Fitted data for the exemplary $Dy(Mn_{0.2}Al_{0.2}Fe_{0.6})_2$ compound

n_1, n_2, n_3	P	W	G (mm/s)	IS (mm/s)	μ_0H_{hf} (T)	QS (mm/s)
0, 0, 6	0.047	0.156(16)	0.170	0.119(11)	19.52(7)	0.007(9)
0, 1, 5 1, 0, 5	0.185	0.217(21)	0.170	0.087(10)	17.10(6)	0.045(8)
0, 2, 4 1, 1, 4 2, 0, 4	0.311	0.20(2)	0.170	0.136(9)	15.00(7)	0.012(7)
0, 3, 3 1, 2, 3 2, 1, 3 3, 0, 3	0.277	0.175(18)	0.170	0.117(12)	12.90(7)	0.035(9)
0, 4, 2 1, 3, 2 2, 2, 2 3, 1, 2 4, 0, 2	0.139	1.142(16)	0.170	0.184(13)	10.01(9)	0.001(10)
0, 5, 1 1, 4, 1 2, 3, 1 2, 4, 0 3, 2, 1 3, 3, 0 4, 1, 1 4, 2, 0 5, 0, 1	0.041	0.110(13)	0.170	0.225(17)	7.25(11)	−0.013(14)
Weighted average values				0.136(8)	14.2(8)	0.018(4)
$\chi^2 = 4.030$				MISFIT = 0.518		

n_1, n_2 and n_3 are the numbers of Mn, Al and Fe atoms, respectively; P and W are probabilities and weights of subspectra, G is 0.5 of the half-width of the Mössbauer line; IS, μ_0H_{hf}, QS are the hyperfine interaction parameters (at 4.2 K).

The fitting procedure of the spectra was carried out analogously as for the series $Dy(Mn_{0.4}Fe_{0.6-x}Al_x)_2$ described previously [16]. The fitted subspectra and the resulting fitted spectrum (lines) are presented in Fig. 3 for each compound of the series studied by Mössbauer effect.

It can be added that the n.n. surrounding is composed of n_1 Mn atoms, n_2 Al atoms and n_3 Fe atoms. The probabilities $P(\{6;\ n_1,\ n_2,\ n_3\})$ of the particular n.n. surroundings were calculated using the Bernoulli formulae [26]. As mentioned above $l = 6$ is the number of n.n. in the transition metal sublattice surrounding the studied Fe atom. Although the number of the probabilities $P(\{6;\ n_1,\ n_2,\ n_3\})$ is quite large, there is a considerable number of the vanishingly small probabilities and these can be neglected during the fitting procedure.

Exemplary fitting results for the compound $Dy(Mn_{0.2}Al_{0.2}Fe_{0.6})_2$ are presented in Table 2. As in the case of the $Dy(Mn_{0.4}Fe_{0.6-x}Al_x)_2$ series it was assumed that the magnetically most important constituents are the Fe atoms [16]. In the table there is presented the probability $P(n_3 = i) = \sum P\{n_1, n_2, n_3 = i\}$, where the summation is taken over the set of numbers $\{n_1, n_2, n_3 = i\}$. As previously, it was assumed during the fitting procedure that the starting amplitudes $A(n_3 = i)$ (and thus the weights of subspectra: $W(n_3 = i) = A(i)/\sum A(k)$) follow the probabilities $P(i)$. Since in the series $Dy(Mn_{0.4-x}Al_xFe_{0.6})_2$ the probability to find an Fe atom in the crystal lattice is constant ($p_3 = 0.6$), the distributions of probabilities $P(i)$ are the same across the series (Fig. 4), within the frame of the used approximation (neglected small probabilities) [26]. The calculated probabilities $P[= P(i)]$ and the fitted weights $W[= W(i)]$ are contained in Table 2. First of all, the table contains the determined hyperfine interaction parameters, i.e. the isomer shift IS (related to pure iron metal at 300 K), the magnetic hyperfine field μ_0H_{hf} and the quadrupole interaction parameter QS (defined in Ref. [27]) and their average values calculated following the formula $X = \sum W(i)X_i/\sum W(k)$.

Actually, it is impossible during the numerical analysis to consider all the factors reflecting the physical complexity of the problem. For instance, the influence of the next nearest neighbor configurations, and a possible deviation from randomness among atoms were not taken into account and thus some arbitrariness of the fitting procedure cannot be avoided. Consequently, some differences between P (open rectangles) and W (shaded rectangles) are observed (Fig. 4). Nevertheless, taking into account the mentioned complexity of the spectra and thus of the fitting procedure, the probabilities P and the weights W seem to be satisfactorily similar.

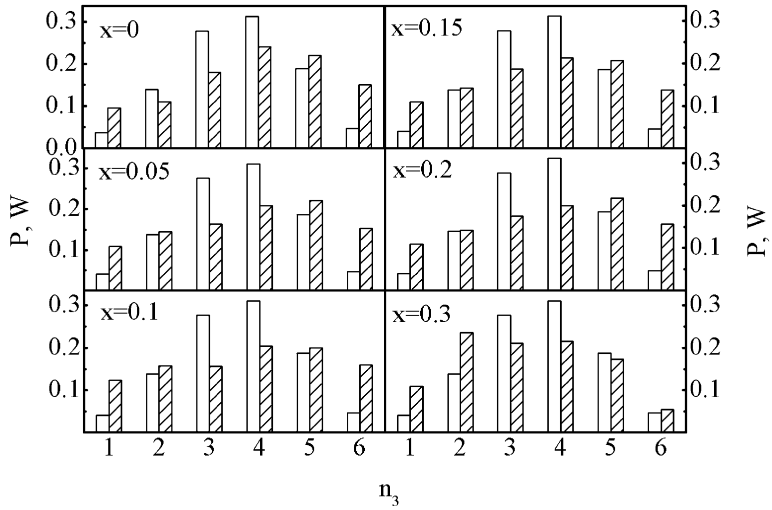

Fig. 4. Probabilities P (open rectangles) and weights W (shaded rectangles) of the particular subspectra against the number n_3 of the Fe atoms as nearest neighbors for the series $Dy(Mn_{0.4-x}Al_xFe_{0.6})_2$.

4. Average hyperfine interaction parameters

The determined average values of the hyperfine interaction parameters of the $Dy(Mn_{0.4-x}Al_xFe_{0.6})_2$ compounds are presented in Fig. 5. Moreover, the values of the parameters are listed in Table 3. Additionally, the previous literature data for $x = 0$ and $x = 0.4$ are included in the figure and the table [13,25].

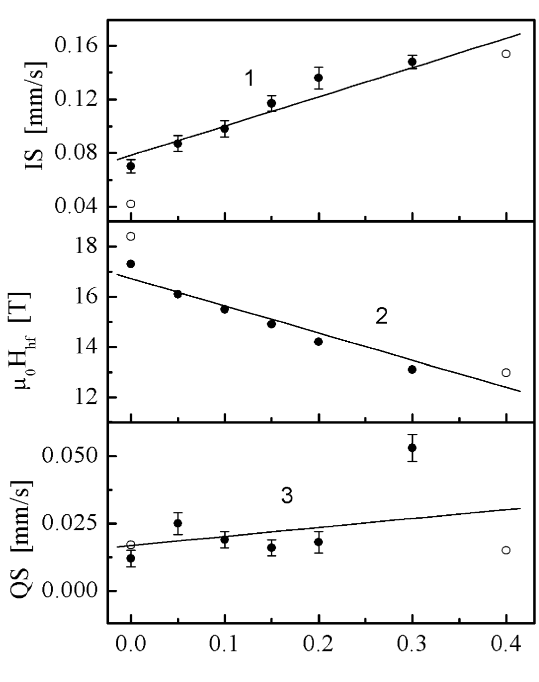

Fig. 5. Average hyperfine interaction parameters of the $Dy(Mn_{0.4-x}Al_xFe_{0.6})_2$ series (4.2 K): (1) the isomer shift IS in relation to Fe metal, 300 K, (2) the magnetic hyperfine field μ_0H_{hf} and (3) the quadrupole interaction parameter QS. Open points after Refs. [13,25].

The average isomer shift IS(x) equals 0.070(5) mm/s at $x = 0$, increases linearly across the series $Dy(Mn_{0.4-x}Al_xFe_{0.6})_2$ and approaches the value 0.148(5) mm/s at $x = 0.3$. Experimental points follow the fitted formula $IS(x) = [0.218(27)x + 0.078(6)]$ mm/s. Considering this formula the extrapolated value of IS, 0.178 mm/s for $x = 0.4$, can be found. This value is relatively close to the IS parameter [=0.154(29) mm/s] known for $Dy(Al_{0.4}Fe_{0.6})_2$ [13]. The mechanism responsible for the change in isomer shift was already discussed in detail elsewhere [10].

The magnetic hyperfine field μ_0H_{hf} equals 17.34(5) T for $Dy(Mn_{0.4}Fe_{0.6})_2$ (this value fits well to the dependence $\mu_0H_{hf}(y)$ observed for the $Dy(Mn_{1-y}Fe_y)_2$ series [6,25]) and decreases considerably with the Al content x to the value 13.1(5) T for $x = 0.3$ and 12.98(70) T for $x = 0.4$ [13]. The line through the experimental points corresponds to a linear fit: $\mu_0H_{hf}(x) = [-10.82(95)x + 16.72(28)]$ T.

The quadrupole interaction parameter QS adopts small values and it is expected that it slightly increases with x, if it varies at all.

5. The branch of the Slater–Pauling curve

The 3d/3d Slater–Pauling curve $\mu_0H_{hf}(n)$, a result of the substitution of one transition metal by the other, observed for the $Dy(M\text{–}M)_2$ compounds (M–M = Mn–Fe, Fe–Co) [5,6] (Fig. 6, line 1; $\mu_0H_{hf} = 12.019(516)n - 49.231(2.971)$, $\mu_0H_{hf} = [-4.14(1.05)n + 51.168(6.781)]$ T), and the $\mu_0H_{hf}(n)$ data of the $Dy(Mn_{0.4}Fe_{0.6-x}Al_x)_2$ series [16] (Fig. 6, line 2; $\mu_0H_{hf} = [0.957(268)n^2 - 4.086(2.369)n + 10.366(5.074)]$ T) are compared with the $\mu_0H_{hf}(n)$ branch (Fig. 6, line 3; $\mu_0H_{hf} = [1.196(163)n^2 - 5.982(1.438)n + 14.044(3.081)]$ T) obtained for the $Dy(Mn_{0.4-x}Al_xFe_{0.6})_2$ series. In the last case, the average number of 3d electrons

Table 3
The average hyperfine interaction parameters (4.2 K) for $Dy(Mn_{0.4-x}Al_xFe_{0.6})_2$

x	n	G (mm/s)	IS (mm/s)	$\mu_0 H_{hf}$ (T)	QS (mm/s)
0 [25]	5.60	0.160; 0.171	0.070(5); 0.042(30)	17.34(6); 18.40(8)	0.012(3); 0.017(8)
0.05	5.35	0.160	0.087(6)	16.13(7)	0.025(4)
0.1	5.10	0.160	0.098(5)	15.54(6)	0.019(3)
0.15	4.85	0.170	0.117(6)	14.92(5)	0.016(3)
0.2	4.60	0.170	0.136(8)	14.24(8)	0.018(4)
0.3	4.10	0.180	0.148(5)	13.09(5)	0.053(5)
0.4 [13]	3.60	0.175	0.154(29)	12.98(70)	0.015(8)

n: average number of 3d electrons; IS: isomer shift; $\mu_0 H_{hf}$: magnetic hyperfine field; QS: quadrupole interaction parameter.

calculated per one site of the transition metal sublattice can be expressed as $n(x) = (0.4 - x) \times 5 + 0.6 \times 6$, where 5 and 6 are numbers of 3d electrons of the Mn and Fe atoms, respectively. As mentioned above, an aluminium atom introduces $3s^2p^1$ electrons instead of the $3d^54s^2$ electrons of the transition metal Mn atom. It can be seen that as a result of the Mn/Al substitution the field $\mu_0 H_{hf}(n)$ creates a new 3d4s/3sp branch which bifurcates from the 3d/3d Slater–Pauling curve. The field of this new branch falls down nonlinearly with decreasing n. Here it should be emphasized that the Fe/Al substitution (Fig. 6, line 2; the series $Dy(Mn_{0.4}Fe_{0.6-x}Al_x)_2$) more strongly reduces the magnetic hyperfine field $\mu_0 H_{hf}(n)$ as compared to the reduction of the field caused by the Mn/Al substitution (Fig. 6, line 3; the series $Dy(Mn_{0.4-x}Al_xFe_{0.6})_2$). The Fe/Al substitution removes one more 3d electron as compared to the Mn/Al substitution, which is the origin of the differences between curves 2 and 3.

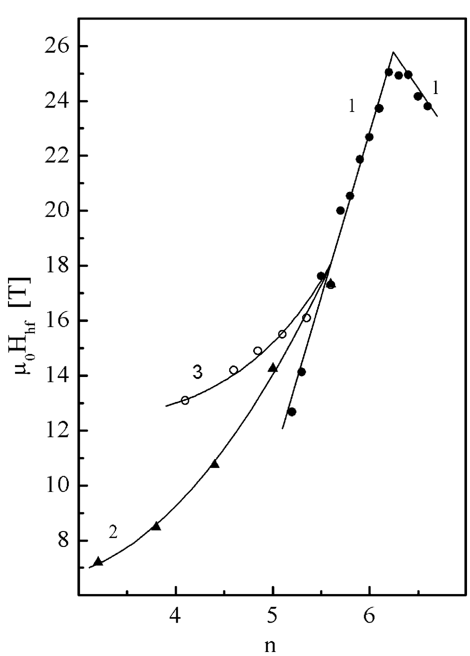

Fig. 6. Magnetic hyperfine fields $\mu_0 H_{hf}(n)$ (4.2 K) compared for series: (1) $Dy(M\text{–}M)_2$ (M–M = Mn–Fe, Fe–Co) [5,6], (2) $Dy(Mn_{0.4}Fe_{0.6-x}Al_x)_2$ [16], (3) $Dy(Mn_{0.4-x}Al_xFe_{0.6})_2$.

6. Summary

The 3d subbands of the starting compound $Dy(Mn_{0.4}Fe_{0.6})_2$ of the $Dy(Mn_{0.4-x}Al_xFe_{0.6})_2$ series are filled-up only partially and both are far away from their completeness. The value of the ^{57}Fe magnetic hyperfine field observed for the $Dy(Mn_{0.4}Fe_{0.6})_2$ belongs to the left branch of the 3d/3d Slater–Pauling curve (Fig. 6, line 1) and lies at a considerable distance from the top area of the $\mu_0 H_{hf}(n)$ fields (curve 1). The Mn/Al substitution in the series $Dy(Mn_{0.4-x}Al_xFe_{0.6})_2$ induces strong changes in the 3d band whereas the contribution of iron remains constant across the series.

As well as for the Fe/Al substitution, the Mn/Al substitution is expected to introduce a number of changes in the 3d band [17,18]. At first, there is no doubt that the Mn/Al substitution should change the Fermi energy, the width of bands and the energy shift between subbands [17,18].

The number of manganese atoms in the transition metal sublattice is reduced with x and simultaneously the $MgCu_2$-type crystal lattice parameter a (Table 1) and thus the distance $d_{M\text{–}M} = a(2)^{1/2}/4$ between the transition metal atoms as nearest neighbors increase. Additionally, the mean distance $D_{M\text{–}M}$ among the statistically distributed transition metal atoms in the crystal lattice increases and the volume w per atom increases. Consequently, as discussed elsewhere [28], the factors of this sort should reduce across the series the overlap of the 3d wave functions of the neighboring transition metal atoms. In effect, the 3d electrons are gradually withdrawn from the band and the 3d electron densities at the iron atoms area increase with x [10,14,29].

It is already known that an increase of the 3d electron density at a given 3d atom (particularly iron atom) leads to a rise of the isomer shift observed at ^{57}Fe [29]. Fig. 7 shows a practically linear correlation between the isomer shift IS(x) and the crystal volume $w(x)$ calculated per atom which supports the above ideas, as discussed elsewhere [12].

The next main problem to discuss below is the $\mu_0 H_{hf}(n)$ dependence. The reduction of the magnetic hyperfine field against the decreasing n (Fig. 6, curve 3) can be qualitatively related to the rigid band model [17,18]. Although the formally calculated number n of 3d electrons per transition metal site decreases with the Al content, it seems that in fact there is no a considerable 3d electron density at the Al

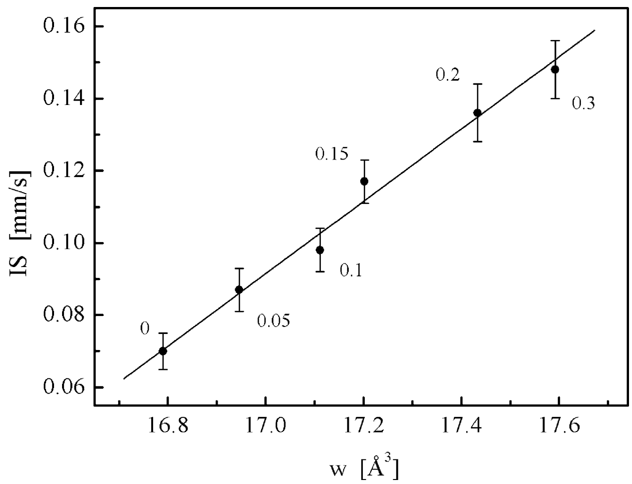

Fig. 7. The correlation between the isomer shift IS and the average volume w per atom for the series $Dy(Mn_{0.4-x}Al_xFe_{0.6})_2$; x-values belonging to the corresponding experimental points are added.

atoms, if any. A similar problem was discussed previously [12]. It seems reasonable to assume that the 3d electrons reside mainly at the transition metal atoms area and that their 3d electron density $\rho_{3d} = \rho^+_{3d} + \rho^-_{3d}$ per atom is presumably constant across the series. The ρ^+_{3d} and ρ^-_{3d} densities correspond to the spin-up and spin-down subbands, respectively.

The Mn/Al substitution reduces the average number u of the magnetic nearest neighbors surrounding the probed Fe atom and thus reduces the energy shift $\Delta E \sim \sum J_{M\text{–}M} m_M$ (summation over magnetic nearest neighbors) between the 3d subbands, where $J_{M\text{–}M}$ is an exchange integral, and presumably also lowers the Fermi level E_F. In effect, the 3d electrons should become gradually redistributed over the 3d subbands and the difference between the ρ^+_{3d} and ρ^-_{3d} densities should become reduced step by step with x. Consequently, the magnetic moment m_M of the 3d atom and thus the magnetic hyperfine field $\mu_0 H_{hf}$ should also decrease and finally the 3d4s/3sp branch of the Slater–Pauling curve is observed (Fig. 6, curve 3). Comparing the magnetic ordering temperature of $DyFe_2$ ($T_C = 635\,K$ [1,2]) and the magnetic ordering temperature of $Dy(Mn_{0.4}Fe_{0.6})_2$ ($T_C = 395\,K$ [30]) it can be concluded that the exchange integral $J_{Fe\text{–}Fe}$ has a considerably higher value as compared to the $J_{Fe\text{–}Mn}$ exchange integral. Thus the reduction of the energy shift ΔE(Mn/Al) caused by the Mn/Al substitution is lower as compared to the reduction of the energy shift ΔE(Fe/Al) enforced by the Fe/Al substitution.

As a result the $\mu_0 H_{hf}(n)$ curve observed for the series $Dy(Mn_{0.4-x}Al_xFe_{0.6})_2$ (Fig. 3, curve 3) is situated above the $\mu_0 H_{hf}(n)$ curve observed for the series $Dy(Mn_{0.4}Fe_{0.6-x}Al_x)_2$ (Fig. 3, curve 2).

Since there is no satisfactory background to predict, for example, the change in position of the subbands in relation to the Fermi level E_F, and the 3d electron densities ρ^+_{3d}, ρ^-_{3d} and ρ_{3d} are unknown yet, at present a more exhaustive discussion is impossible. In fact, the electronic structures of certain rare earth–transition metal compounds were previously studied theoretically and numerically and the band structures were proposed, for instance, in Refs. [31–33]. However, the systematic theoretical and numerical studies of the band structure of the 3d/3d substituted series and especially of the new 3d4s/3sp substituted series are unknown yet. Thus for a more precise discussion, a knowledge of the band structure of the Al-substituted intermetallic series is necessary. For this purpose future sound theoretical and numerical studies would be helpful.

Acknowledgements

Supported partially by Polish Committee of Scientific Studies, grant No. 4T08D03322. M. Mróz and T. Winek are acknowledged for technical assistance.

References

[1] K.N. R Taylor, Adv. Phys. 20 (1971) 551.
[2] K.H.J. Buschow, in: E.P. Wohlfarth (Ed.), Ferromagnetic Materials, vol. 1, North-Holland, Amsterdam, 1980.
[3] E. Burzo, H.R. Kirchmayr, in: K.A. Gschneidner Jr., L. Eyring (Eds.), Handbook on the Physics and Chemistry of Rare Earths, vol. 12, North-Holland, Amsterdam, 1989.
[4] I.A. Campbell, J. Phys. F: Metal Phys. 2 (1972) L47.
[5] B. Gicala, J. Pszczoła, Z. Kucharski, J. Suwalski, Phys. Lett. A 185 (1984) 491.
[6] B. Gicala, J. Pszczoła, Z. Kucharski, J. Suwalski, Solid State Commun. 96 (1995) 511.
[7] C.E. Johnson, M.S. Ridout, T.E. Cranshaw, Phys. Rev. Lett. 6 (1961) 450.
[8] C.E. Johnson, M.S. Ridout, T.E. Cranshaw, Proc. Phys. Soc. 81 (1963) 1079.
[9] R.M. Bozorth, Ferromagnetism, Van Nostrand, Princeton, 1968.
[10] H. Maletta, G. Crecelius, W. Zinn, J. de Phys. Suppl. 35 (1974) C-6-279.
[11] J. Bara, A. Pędziwiatr, W. Zarek, D. Konopka, U. Gacek, J. Magn. Magn. Mater. 27 (1982) 159.
[12] J. Pszczoła, B. Winiarska, J. Suwalski, Z. Kucharski, J. Alloys Comp. 265 (1998) 15.
[13] J. Pszczoła, B. Gicala, J. Suwalski, J. Alloys Comp. 274 (1998) 47.
[14] J. Pszczoła, J. Żukrowski, J. Suwalski, Z. Kucharski, M. Łukasiak, J. Magn. Magn. Mater. 40 (1983) 197.
[15] A. Ślebarski, J. Less-Common Met. 72 (1980) 231.
[16] P. Stoch, J. Pszczoła, P. Jagodziński, A. Jabłońska, J. Suwalski, L. Dąbrowski, A. Pańta, J. Alloys Comp. 375 (2004) 24.
[17] J.M. Ziman, Principles of the Theory of Solids, Cambridge University Press, London, 1972.
[18] W. Vonsovskij, Magnetism, Nauka, Moscow, 1971 (in Russian).
[19] H.M. Rietveld, J. Appl. Cryst. 2 (1969) 65.
[20] J. Rodriguez-Carvajal, Physica B 192 (1993) 55.
[21] F. Laves, Naturwissenschaften 27 (1939) 65.
[22] J. Chojnacki, Structural Metallography, Śląsk Press, Katowice, 1966.
[23] Z. Bojarski, E. Łągiewka, Röntgen Structural Analysis, Silesian University Press, Katowice, 1995 (in Polish).
[24] J. Pszczoła, A. Feret, B. Winiarska, L. Dąbrowski, J. Suwalski, J. Alloys Comp. 299 (2000) 59.
[25] B. Gicala, J. Pszczoła, Z. Kucharski, J. Suwalski, Nukleonika 39 (1994) 195.

[26] W. Feller, An Introduction to Probability Theory and Its Applications, Wiley, New York, 1961.
[27] G.K. Wertheim, Mössbauer Effect, Academic Press, London, 1964.
[28] K.H.J. Buschow, J. Less-Common Met. 43 (1975) 55.
[29] F. van der Woude, G.A. Sawatzky, Phys. Rep. 12 (1974) 335.
[30] J. Pszczoła, J. Suwalski, Mol. Phys. Rep. 22 (1998) 41.
[31] R. Coehoorn, J. Magn. Magn. Mater. 99 (1991) 55.
[32] R. Coehoorn, K.H.J. Buschow, J. Magn. Magn. Mater. 118 (1993) 175.
[33] R.F. Sabirianov, S.S. Jaswal, J. Appl. Phys. 79 (1996) 5942.